Topic area: **CMMSP**

Elastic modulus of silicon nitride thin films from nanoindentation

M. T. K. Soh[1,2], A. C. Fischer-Cripps[2], N. Savvides[2], C. A. Musca[1], J. M. Dell[1] and L. Faraone[1]

[1]*School of Electrical, Electronic and Computer Engineering, The University of Western Australia, Crawley 6009*
[2]*CSIRO Industrial Physics, Lindfield 2070*

e-mail of corresponding author: msoh@ee.uwa.edu.au

Introduction

Plasma-deposited *amorphous* silicon nitride (a–SiN_xH_y) thin films and similar materials are increasingly being used as flexible membranes in micro-systems-technology [1–3]. Currently, there is a need to improve on or develop new methods to characterise the mechanical properties of such films. This is because traditional methods such as bulge and tensile testing are impratical and/or unsuitable, since they do not scale well into the micro and nano-scale. Nonetheless, the advent of nanoindentation instruments, and subsequent development of its underlying science may potentially address the scaling problem. Although the elastic contact problem, which plays a key part in the analysis of the compliance data, was originally considered by Boussinesq and Hertz in the late 19th century, it was not possible until recently to extract from nanoindentation desirable physical properties such as Young's modulus [4–6].

In this work, we report nanoindentation measurements on a–SiN_xH_y thin films that are under compressive and tensile strain. We demonstrate that the multi-point unload technique [5], commonly used to calculate the contact area, gives modulus values which differ significantly from values that are determined using the true contact area on the film surface obtained by atomic force microscope (AFM).

Experiment

The a–SiN_xH_y thin films ($\sim$ 800 nm thick) were deposited at various temperatures (T_d) in the range 150–300 °C, using plasma-enhanced chemical-vapour-deposition [7]. This process allowed films to be deposited which had residual strain (ε) at 20 °C from compressive ($\varepsilon = -1.6 \times 10^{-3}$) to tensile ($\varepsilon = 0.9 \times 10^{-3}$) (on single-crystal [100] germanium (Ge) and silicon (Si) substrates). A CSIRO UMIS II nanoindentation system with a calibrated Berkovich diamond indenter was used to perform the nanoindentation at room temperature (20 °C). Images of the residual impressions were recorded with an AFM (DME DualScope 45-40) attachment.

For the purposes of this analysis, the unload stiffness (S) and projected contact depth (h_p) were calculated through the commonly used multi-point unload technique [5]. These parameters yield closed-form expressions for reduced modulus ($\left(E_f^{*-1} + E_i^{*-1}\right)^{-1} \equiv S\sqrt{\pi/A}/(2\beta)$). Here, P is the maximum load, E_f^* is the plane-strain modulus, E_i^* ($= 1005$ GPa) is the indenter tip plane-strain modulus, A is the contact area, and β is a correction factor to account for

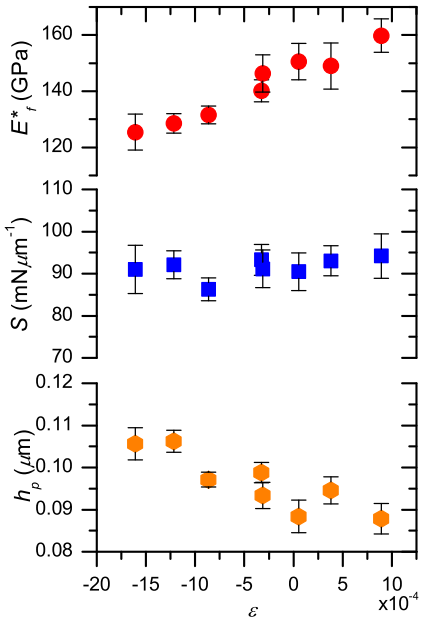

Figure 1: E_f^*, S and h_p, *vs.* ε. The errorbars denote the standard deviation of each data point.

indenter asymmetry. $E_f^*\left(h_t/h_f\right) \equiv E/\left(1-\upsilon^2\right)$, where h_t is the total indentation depth, h_f is the thin film thickness, h_t/h_f is the normalised indentation depth, E is a thin film elastic modulus, and υ is a thin film Poisson ratio. For an ideal Berkovich indenter, the projected contact area $A\left(h_p\right) \equiv 24.5h_p^2$.

Results and discussion

Figure 1 shows the variation of the parameters E_f^*, S and h_p, with ε for the range of thin films studied. The data was computed from 10 indentations at 5 mN load ($h_t/h_f \approx 0.1$). Note that ε was calculated from an earlier study [7]. It is clear that E_f^* monotonically increases with increasing residual strain, regardless of the thin film deposition temperature. The results suggest that E_f^* is dependent on ε, although S indicates no dependence. The h_p data may provide a reason for this disrepancy. Its monotonic decrease with residual strain suggests that the projected contact area of indented *a*–SiN_xH_y thin films under tensile residual strain is lower.

To resolve this problem, we consider the actual contact area, which may be determined from AFM imaging of the residual indentation imprint (Figure 2). Image processing consisted of automatic 3-point levelling of the scan topography using the vendor-supplied software, and area calculation by pixel counting using ImageJ software. The imprint boundaries were verified by using the linescan tools provided in the former. From Figure 2, it is clear that there is some degree of elastic recovery. This means that calculations of $E_f^*\left(h_t/h_f\right)$ based on the *P*–*h* data alone may be wrong, since the indenter contact area is used in the analysis [5]. McElhaney *et al.* [8] suggested a technique based on a tip calibration factor corrected for such effects. However, such a method may not be practical since *a priori* knowledge of $E_f^*\left(h_t/h_f\right)$

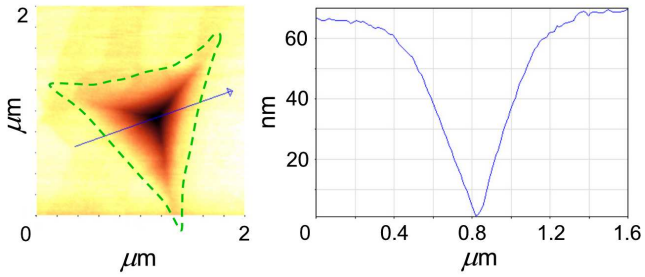

Figure 2: AFM image and cross-section profile for a a–SiN_xH_y thin film on Ge ($T_d = 300$ °C, $P = 35$ mN). The dashed enclosed area is the measured indentation area, A_{AFM}.

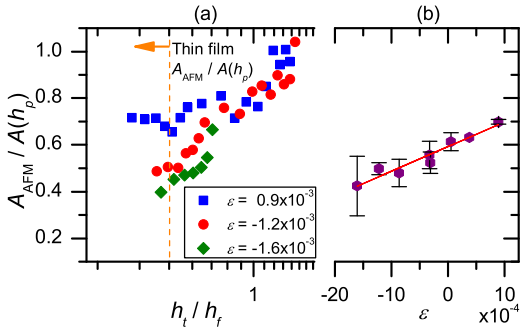

Figure 3: (a) $A_{\mathrm{AFM}}/A(h_p)$ for a–SiN_xH_y thin film specimens, with tensile ($\varepsilon = 0.9 \times 10^{-3}$, $T_d = 300$ °C, on Si) and compressive ($\varepsilon = -1.2 \times 10^{-3}$, $T_d = 150$ °C, on Si; -1.6×10^{-3}, 150 °C, on Ge) strain. (b) $A_{\mathrm{AFM}}/A(h_p)$ *vs.* ε for each a–SiN_xH_y thin film specimen; the errorbars denote the standard deviation of each datapoint, and the solid line is a least-squares linear fit to the data.

is required, which for a–SiN_xH_y is generally unknown.

Figure 3(a) shows the ratio of AFM contact area (A_{AFM}) and $A(h_p)$ for three specimens: one with tensile and two with compressive strain. For larger loads, $A_{\mathrm{AFM}}/A(h_p) \rightarrow 1$ since the plastic zone is driven deeper into the substrate. It also appears that $A_{\mathrm{AFM}}/A(h_p)$ has a lower limit at low loads, which we will define as the thin film $A_{AFM}/A(h_p)$. The solid line is a least-squares linear fit to the data, and serves to highlight the impact of residual strain on the degree of elastic recovery. Briefly, during nanoindentation, an indenter force is applied perpendicular to the thin film/substrate. Tensile residual strain in the film increases the shear stress, and since shear stress controls plastic deformation, the indentation plasticity is enhanced [9]. Therefore, $A_{\mathrm{AFM}}/A(h_p)$ will be larger than in the absence of this strain. Conversely, thin films with compressive strain will have lower shear stress beneath the indenter, which permits elastic recovery, and yields a lower contact area. E_f^* calculated from A_{AFM} (Figure 4) are similar to other reported values for silicon nitride thin films [10, 11].

Conclusion

Nanoindentation was used to investigate a–SiN_xH_y thin films of variable ε between -1.6×10^{-3} and 0.9×10^{-3}. H and E_f^* calculated using the multi-point unload technique [5]

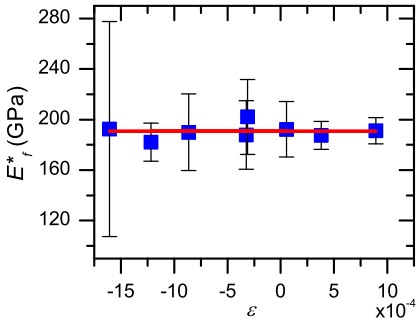

Figure 4: a–SiN_xH_y thin film E_f^*, *vs.* ε calculated using A_{AFM}. The solid line in each plot denotes the average value of the data.

was observed to be dependent on ε. However, AFM imaging of the residual impressions on the thin film surface indicates some degree of elastic recovery. The degree of elastic recovery was found to be dependent on ε, with thin film $A_{\mathrm{AFM}}/A\left(h_p\right)$ monotonically increasing with ε. E_f^* calculated using A_{AFM} was independent of ε, and approximately 190 GPa. Since strain is present in most thin films and multilayers, often due thermal mismatch, imaging of residual impressions is necessary in order to measure the actual contact area, and so accurately determine the Elastic modulus of thin films using nanoindentation.

Acknowledgements

This work was financially supported by the Australian Research Council and the CSIRO.

[1] T. Giesler and J.-U. Meyer, Sens. Actuators B, Chem. **B18**, 103 (1994).
[2] P. R. Scheeper, W. Olthuis, and P. Bergveld, J. Micromech. Microeng. **2**, 187 (1992).
[3] D. Memmi, V. Foglietti, E. Cianci, G. Caliano, and M. Pappalardo, Sens. Actuators A, Phys. **99**, 85 (2002).
[4] M. F. Doerner, D. S. Gardner, and W. D. Nix, J. Mater. Res. **1**, 845 (1986).
[5] W. C. Oliver and G. M. Pharr, J. Mater. Res. **7**, 1564 (1992).
[6] J. S. Field and M. V. Swain, J. Mater. Res. **8**, 297 (1993).
[7] M. T. K. Soh, C. A. Musca, N. Savvides, J. M. Dell, and L. Faraone, J. Microelectromech. Syst. (submitted).
[8] K. W. McElhaney, J. J. Vlassak, and W. D. Nix, J. Mater. Res. **13**, 1300 (1998).
[9] A. Bolshakov, W. C. Oliver, and G. M. Pharr, J. Mater. Res. **11**, 760 (1996).
[10] J. J. Vlassak and W. D. Nix, J. Mater. Res. **7**, 3242 (1992).
[11] T.-Y. Zhang, Y.-J. Su, C.-F. Qian, M.-H. Zhao, and L.-Q. Chen, Acta Mater. **48**, 2843 (2000).